

# Monitoring and Controlling the Dissolved Oxygen (DO) Concentration within the High Aspect Ratio Vessel (HARV)

Mark A. Saarinen,<sup>†</sup> Julie S. Reece,<sup>‡</sup> Mark A. Arnold,<sup>‡</sup> and David W. Murhammer<sup>\*,†</sup>

Departments of Chemical and Biochemical Engineering and Chemistry, University of Iowa, Iowa City, Iowa 52242

A probe-type oxygen sensor was developed utilizing a radioluminescent (RL)-based light source and a ruthenium-based sensing chemistry for monitoring the dissolved oxygen (DO) concentration in a modified version of the NASA-designed high aspect ratio vessel (HARV), a batch rotating wall vessel. This sensor provided the means to monitor the DO concentration in the HARV without influencing the flow pattern, thereby retaining the low shear HARV environment conducive to the formation of 3-dimensional cell aggregates. This sensor lost significant signal as a result of exposure to the first three autoclave cycles, but only minimal change in signal was observed following exposure to subsequent autoclave cycles. A new calibration model requiring only one fitted parameter was developed that accurately fit data over the entire range from 0% to 100% oxygen saturation. The ability for DO concentration control within the vessel was demonstrated by using this sensor to monitor the DO concentration inside the HARV.

## Introduction

Bioreactors are widely used for cultivating mammalian, insect, and microbial cells in the mass production of useful products, e.g., antibiotics, fermentation products, and recombinant proteins. Another important application of bioreactors is to simulate *in vivo* conditions for the growth of cells and tissues, thereby providing an *in vitro* laboratory method for addressing fundamental biomedical questions. Proper *in vivo* simulation requires both formation of three-dimensional cell aggregates to allow crucial cell–cell interactions and the strict control of environmental conditions. The rotating wall vessel (RWV) developed by NASA researchers provides a low shear environment allowing for three-dimensional (3-D) cell aggregate growth. Many investigators have demonstrated the formation of 3-D cell aggregates in the RWV. Recent examples include epidermal growth factor-responsive murine neural precursor cells (1), osteoblast cell cultures (2), and cocultures of pig islets and rat Sertoli cells (3).

In addition to 3-D cell aggregate growth, proper *in vivo* simulation requires a well-controlled environment within the RWV that is representative of the *in vivo* environment. Realization of this goal requires sensing technology providing *in situ* analytical information in a real-time and continuous manner that can then be used for environmental control. One of these critical environmental parameters is the dissolved oxygen (DO) concentration. A radioluminescent (RL)-based flow-through sensor utilizing ruthenium-based sensing chemistry was recently developed for use with perfusion RWVs (4, 5). An RL light source and ruthenium-based sensing chemistry have been utilized to develop a probe-type DO sensor for use

with a batch RWV, i.e., the high aspect ratio vessel (HARV) as described herein. Another issue that has been addressed is designing the HARV and control system to minimize the DO concentration heterogeneities inherent within this low shear bioreactor while maintaining an environment conducive to the formation of 3-D cell structures.

The major advantage of the resulting RL-based oxygen sensor compared to traditional oxygen sensors utilizing an amperometric configuration is that it provides long-term stability and retains its calibration through autoclaving. The major advantage of the RL source compared to LED sources used in other oxygen sensors utilizing fluorescence-based sensing chemistry (6) is the stability of the radiant power. On the time scale of the measurements, RL sources are essentially noise-free. This results in a situation that is detector-noise-limited. Detector noise can be reduced considerably by various hardware and software filtering methods. The RL source also lacks significant drift over a period of days, which is much better than LED sources that can drift over periods of hours. The major limitation of commercially available RL sources is their low radiant powers. The amount of light generated is directly proportional to the amount of radioactivity contained within the source body. The magnitude of radioactivity is limited for safety reasons. The limited radiant powers demand high detector gains in order to detect the resulting luminescence. It is interesting to note that despite the low incident radiation provided by the RL sources, low oxygen levels can be measured because of the noiseless nature of the source. Basically, the signal-to-noise ratio is high because the noise level is extremely low.

## Materials and Methods

**HARV Design.** The existing HARV design developed by NASA researchers (commercially available from Synthecon, Inc., Houston, TX) was modified to provide the

\* To whom correspondence should be addressed. Ph: (319) 335-1228. Fax: (319) 335-1415. Email: murham@engineering.uiowa.edu.

<sup>†</sup> Department of Chemical and Biochemical Engineering.

<sup>‡</sup> Department of Chemistry.

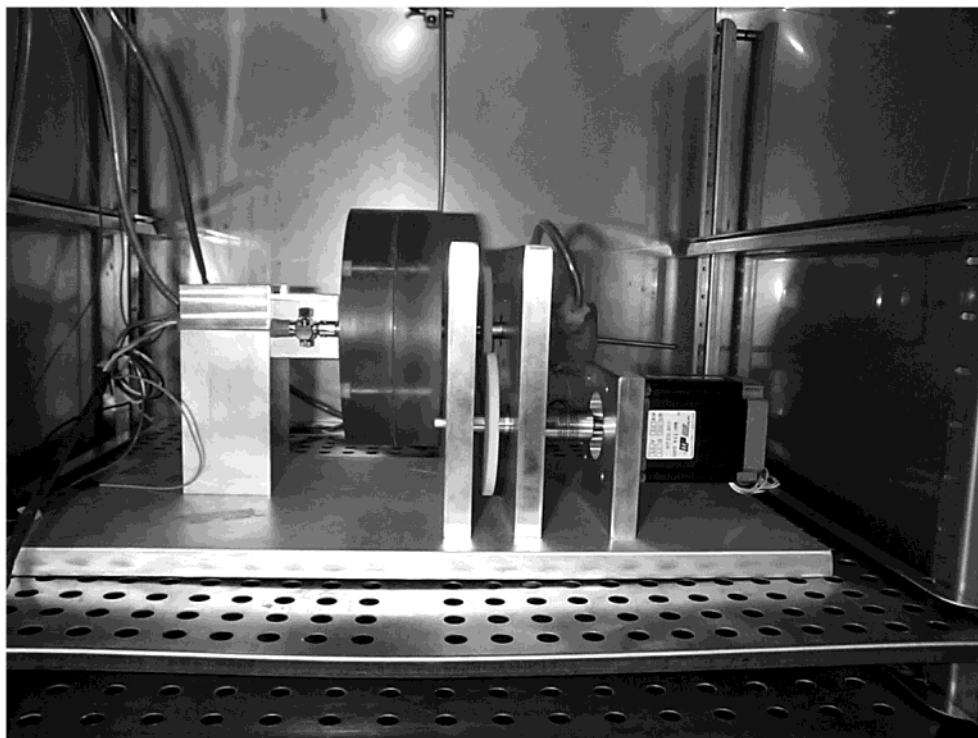


**Figure 1.** Side view of HARV system in incubator with oxygen sensing unit in place.

means to monitor and control the DO concentration. First, a torus-shaped gas pocket extending to the outside edge of the culture chamber was created behind the silicone membrane to facilitate more efficient gas exchange. Second, a 0.866-in. diameter hole was drilled through the center of the front face of the vessel (i.e., the face opposite the silicone membrane) to accommodate introduction of the oxygen sensor (details of this sensor are provided in the next section). Third, a reversible motor (HT23-401 stepper motor; Applied Motion Products, Inc., Watsonville, CA) was used to provide the option of reversing the rotation direction, thereby providing the means to introduce some mixing within the vessel to enhance oxygen transport. Fourth, the system was interfaced with a computer, thereby providing the means for monitoring and controlling the DO concentration within the HARV.

Aside from addressing the issues discussed above, the design for the new HARV culture vessel retained the same physical dimensions of the existing vessel, i.e., an interior cylindrical culture chamber with a diameter and depth of 10 and 0.7 cm, respectively (volume = 55 mL). The vessel and membrane were constructed of Lexan grade 104 plastic (Professional Plastics, San Jose, CA) and biomedical grade reinforced silicone sheeting, 40 durometer, 0.007 in thickness (Specialty Manufacturing Inc., Saginaw, MI), respectively. An O-ring groove was cut into the material surrounding the culture chamber to house a silicone rubber O-ring to seal the front and back portions of the assembled vessel. Two luer ports opening into the interior of the HARV were placed on the front face of the vessel. These ports were located at the same diameter on opposite sides of the vessel center. A hole was drilled through the axis of the rotating shaft to which the vessel is coupled to provide the means for introducing gas (pure O<sub>2</sub> and/or air) to the gas pocket located behind the membrane.

A stand was constructed of heavy aluminum plate to hold components of the system together. Bearings were set into two vertical plates of this stand to support a

rotating shaft. The end of this shaft opposite the vessel was set into a gas mixing chamber constructed of Lexan 104 plastic and rotated in an O-ring seal inserted in the mixing chamber wall. The gas mixing chamber ( $V = 0.6$  mL) was provided with two inlet ports for gas introduction. Another shaft was connected to the motor on one end and a gear constructed of Delrin plastic on the other end. This gear was used to drive a second Delrin plastic gear attached to the shaft that rotates the HARV, thereby providing a coupling between the motor and the HARV. Bearings, gears, and shaft coupling were purchased from W. M. Berg, Inc. (East Rockaway, NY). The motor was mounted behind the two vertical support plates. The modified HARV is shown in Figure 1.

**DO Sensor Design.** An oxygen sensor in a probe-type configuration was designed to monitor the DO concentration based on the fluorescence quenching of tris(4,7-diphenyl-1,10-phenanthroline)ruthenium(II) chloride (Ru(dpp)<sub>3</sub>Cl<sub>2</sub>) by molecular oxygen. The mechanism by which this chemistry functions for the detection of DO concentration is described elsewhere for an analogous flow-through sensor design (4). Although potentially adaptable for use in the HARV, high quality commercially available DO probes are large and less convenient to use. The methodologies used to incorporate the RL-based light source and fluorescence quenching technology into a probe-type configuration are described herein.

The DO probe was designed in two parts, a removable headpiece containing the sensing chemistry and a body containing the electronics. The body of the headpiece was manufactured from a 1-in. diameter 316 stainless steel rod. A hole was bored into the top of the rod to create a shelf to support the glass disk coated with the sensing chemistry. A removable cover was designed to hold the glass disk in place and to seal against leakage. A hole was bored in the bottom of the rod to create a stop for the electronics components inserted into the headpiece when the unit is assembled. The top section of the rod was machined to an outside diameter of 0.850 in. with two grooves around its circumference into which silicone

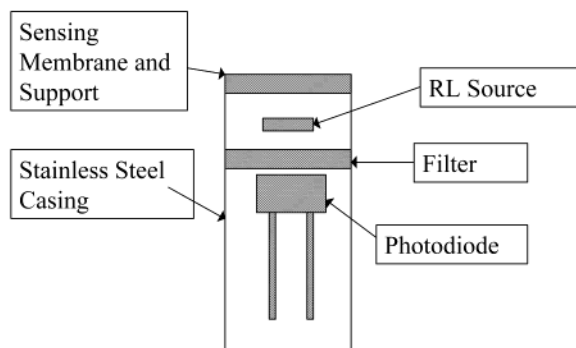


**Figure 2.** Schematic of interior of oxygen sensor for the HARV.

rubber O-rings are placed. When inserted into the hole on the front face of the HARV vessel, a rotating O-ring seal is formed, allowing the oxygen sensor to remain stationary as the vessel rotates. Upon insertion into the HARV vessel, the front face of the probe seals flush with the front face of the interior cell culture chamber; thus, the probe does not alter the flow pattern within the HARV. The bottom section of the rod was threaded to attach to the body of the oxygen sensor, with an O-ring used to seal against moisture.

The sensing portion of the DO probe was prepared by the sequential application of two casting solutions onto glass disks. The first casting solution was prepared from 0.3 mL of 1 mM tris(4,7-diphenyl-1,10-phenanthroline)-ruthenium(II) chloride in methylene chloride (7), 0.15 g of optically transparent acetic acid releasing silicone prepolymer (Dow Corning, Midland, MI), and 0.025 g of titanium dioxide powder (99.9% pure, diameter < 5  $\mu\text{m}$ ; Aldrich Chemical Co., Milwaukee, WI). This casting solution was used to coat glass disks and allowed to cure for 24 h. A second casting solution, prepared from 0.01 g of carbon black (Fisher Chemical, Fairlawn, NJ), 0.12 g of silicone prepolymer, and 0.25 mL of toluene (Fisher Chemical, Fairlawn, NJ), was used to coat the first layer and allowed to cure for 24 h. This second layer protects the first layer from loss of chemical components and shields the  $[\text{Ru}(\text{dpp})_3]^{2+}$  complexes from exposure to outside light. The thickness of each layer was 150  $\mu\text{m}$  prior to drying.

A rectangular box was manufactured from aluminum to house the electronics portion of the oxygen probe. A circuit board containing the electronic components for signal amplification was attached within an interior chamber of this piece. Threaded holes were placed in the front and back of this piece. A photodiode (Hamamatsu, Bridgewater, NJ) was extended from the front and was coupled with a 590-nm-cutoff long pass filter and a disk containing a tritium-based light source. The light source (MB-Microtec, North Tonawanda, NY) produces a faint blue light with emission centered at 450 nm that is used to excite the  $[\text{Ru}(\text{dpp})_3]^{2+}$  complexes embedded in the silicone polymer layer. The cutoff filter is used to shield the photodiode from the excitation radiation produced by the RL source and from stray light in this chamber. Luminescence from the excited  $[\text{Ru}(\text{dpp})_3]^{2+}$  complex is centered at 620 nm and is transmitted through the filter to the detector photodiode. A schematic of the interior of the oxygen sensor is shown in Figure 2. A hermetically sealed connector (PAVE Technology, Inc., Dayton, OH) enclosing wiring connected to the circuit board was screwed into the back of the sensor body. The top of the sensor body was sealed with a flat cover and silicone rubber O-ring. A stand was manufactured from alumi-

num to hold the oxygen sensing unit firmly in place when it is inserted into the HARV vessel. It was attached to the main system stand and located directly in front of the vessel.

**Control System.** The control system consists of several parts, including (i) a control unit for vessel rotation, (ii) mass flow controllers for gas flow to the vessel, and (iii) a computer and software coupled with instrumentation for sending and receiving electrical signals and for data acquisition and process control capabilities. The unit for vessel rotation control consists of a 3540 MO step motor driver (Applied Motion Products, Inc., Watsonville, CA) that is capable of microstep control (12,800 steps/revolution), directional control, and speed sensing and can be interfaced with a computer. The computer (Dell personal computer, Rock Round, TX) was fitted with a board for data acquisition and control (AT-MIO-16E-10) and connected to an external BNC board to which signal wires were attached. Labview software was used as the basis for data acquisition and control. The boards and Labview software were purchased from National Instruments (Austin, TX). During a cell culture run, the signal output by the oxygen sensor is sent to the computer where it is converted to a DO concentration. This information is then used by a process control program to determine the actions to be taken based on the DO concentration setpoint. Signals are then sent to two mass flow controllers (Aalborg Instruments, Orangeburg, NY) where one controls the flow rate of air and the other controls the flow rate of pure  $\text{O}_2$ . These controllers are used to control the oxygen concentration delivered to the gas pocket behind the silicone membrane of the HARV, thereby providing a basis for controlling the DO concentration within the HARV.

**DO Sensor Calibration.** A calibration chamber was assembled from a 1-L glass vessel with a curved bottom and a flat top. A glass cylinder leading into the vessel interior was attached to the side to accommodate the oxygen sensor. The O-rings present on the head of the sensor sealed the system against fluid leakage when inserted into this cylinder. The vessel was covered with a flat steel plate and sealed by an O-ring. A sintered glass sparger was fitted in the center of the cover plate and extended down into the vessel interior. Two small ports were provided on the cover plate for pressure relief. During calibration, the vessel was filled with 1 L of fluid and gas was introduced through the sparger. A magnetic stirring bar was added to the vessel to provide agitation. The sensor was calibrated by filling this chamber with distilled water and sparging with pre-prepared gas mixtures containing known percentages of oxygen for sufficient time to obtain equilibrium. Specifically, calibrations were carried out at 0%, 3.5%, 7.0%, 10.5%, 14.0%, 17.5%, and 100% oxygen saturation. The gases used for the 0% and 100% values were pure  $\text{N}_2$  and pure  $\text{O}_2$ , respectively. Greater detail was paid to the lower range of oxygen concentrations because these values are of particular interest to the monitoring of biological systems.

**Cell Culture Methods.** The *Spodoptera frugiperda* Sf-9 insect cell line was obtained from Gibco-BRL (Grand Island, NY) and was grown in Sf-900 II serum-free medium (Gibco-BRL). Cells grown in shaker flasks were used to seed the HARV at a cell density of  $\sim 10^6$  cells/mL. The HARV was placed in an incubator containing a small cooling fan to enhance heat transfer. Prior to the use of this cooling fan it was found that the temperature within the HARV was several degrees higher than the incubator setpoint temperature. This was believed to

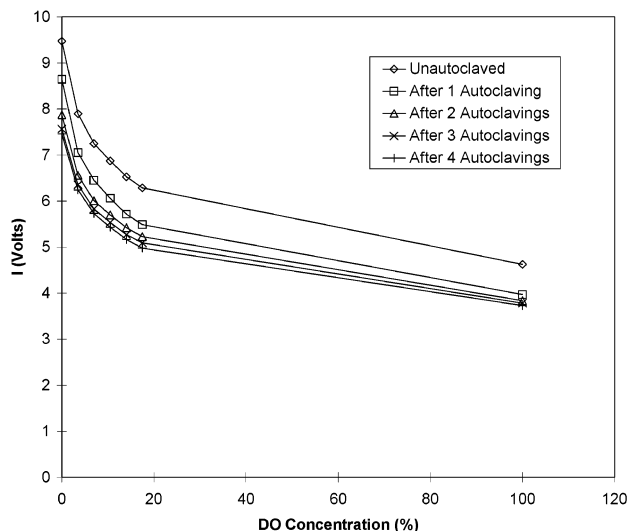


**Figure 3.** Effect of autoclaving on the oxygen sensor. The signal from the oxygen sensor for calibrations carried out over the complete range of DO concentrations is shown.

have resulted from heat generated by the motor. Cell growth was conducted at 27 °C in all of these experiments.

## Results and Discussion

**Effect of Autoclaving on Sensor Performance.** A series of calibration tests was carried out at 23 °C to determine the effects of autoclaving the sensor headpiece, which contains the oxygen sensing chemistry. Measurements focused on the stability of the signal produced when exposed to different DO concentrations. It is important to note that temperature has a significant effect on the fluorescence quenching of Ru(II)-based metal–ligand indicator complexes (8, 9). Therefore, care must be taken to carry out calibrations at constant temperature. Also, prior to use, the calibration needs to be carried out at the temperature at which the oxygen sensor is to be used. Calibration was performed prior to and following autoclave cycles of 30 min duration at 125 °C. The results (Figures 3 and 4) show a significant loss of signal after one autoclave cycle, an additional noticeable decline from one to two cycles, and a much smaller decline from two to three cycles. The signal after four autoclave cycles is very similar to that after three cycles, with the difference at any calibration point being less than 2%. The reason for the observed loss of signal may be the effect of additional curing of the polymer support matrix that increases its opacity. These results are consistent with previous findings demonstrating that fluorescent-based dissolved gas sensors can be autoclaved (6, 10).

**Calibration Modeling.** The Stern–Volmer equations, commonly used to model purely dynamic fluorescence quenching of fluorescent complexes in a homogeneous environment, are given by

$$\frac{I_0}{I} = 1 + K_{sv}[Q] \quad (1)$$

and

$$\frac{\tau_0}{\tau} = 1 + K_{sv}[Q] \quad (2)$$

where  $I$  is the luminescent intensity,  $\tau$  is the luminescent

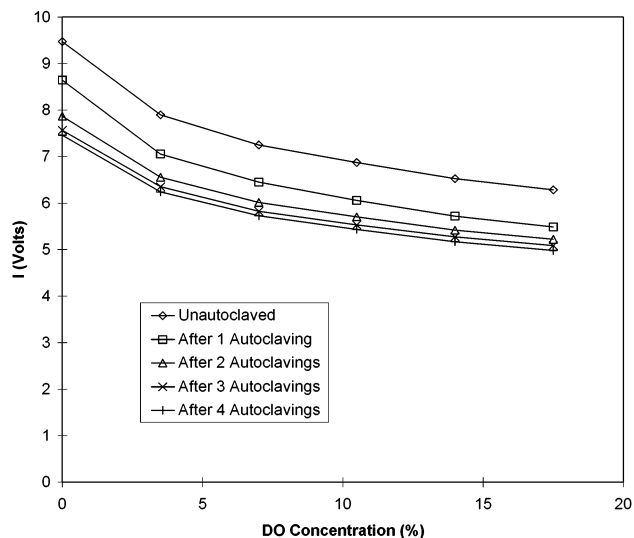


**Figure 4.** Effect of autoclaving on the oxygen sensor. The signal from the oxygen sensor for calibrations carried out over the lower range of DO concentrations is shown.

lifetime,  $K_{sv}$  is the Stern–Volmer quenching constant and is equal to  $k_q\tau_0$ ,  $[Q]$  is the concentration of the quencher,  $k_q$  is the bimolecular quenching rate constant, and the subscript 0 denotes values present in the absence of quencher. On the basis of this model, a plot of  $I_0/I$  vs  $[Q]$  should be linear for dynamic quenching in a homogeneous matrix. However, studies of the fluorescence quenching of metal–ligand complexes dispersed in polymer matrices have found such plots to be nonlinear. As a consequence, this model is unsatisfactory to describe the resulting oxygen quenching of  $[\text{Ru}(\text{dpp})_3]^{2+}$  fluorescence. Explanations for this nonlinearity include (i) the polymer support matrix is heterogeneous when considered on a microscopic level, (ii)  $[\text{Ru}(\text{dpp})_3]^{2+}$  exists in the matrix in both freely dissolved and aggregated forms, and (iii) some static quenching occurs (11–17).

Moreno-Bondi et al. (18) suggested a modification of the Stern–Volmer equation (eq 1), in which background light not associated with quenchable indicator fluorescence is removed. This modified equation is given by Chuang and Arnold (4) as

$$\frac{I_0 - I_{NQ}}{I - I_{NQ}} = 1 + K_{sv}[Q] \quad (3)$$

where  $I_{NQ}$  is the amount of signal not quenchable by DO in solution or the intensity measured at 100% DO concentration. The other elements of the equation have the same meaning as in eq 1. Equation 3 will subsequently be referred to as Model 1.

Our calibration data demonstrated a strong linearity between the signal and the natural logarithm of the DO concentration. From this observation, the following equation was proposed:

$$I = k \ln[Q] + R \quad (4)$$

where  $k$  and  $R$  are empirical constants obtained from curve fitting. The other elements of the equation have the same meaning as in eq 1. Equation 4 will subsequently be referred to as Model 2.

The ability of Models 1 and 2 to fit the actual oxygen sensor calibration after four autoclave cycles is shown in Figures 5 and 6. Figure 5 plots the signals calculated by Models 1 and 2 as a function of DO concentration for

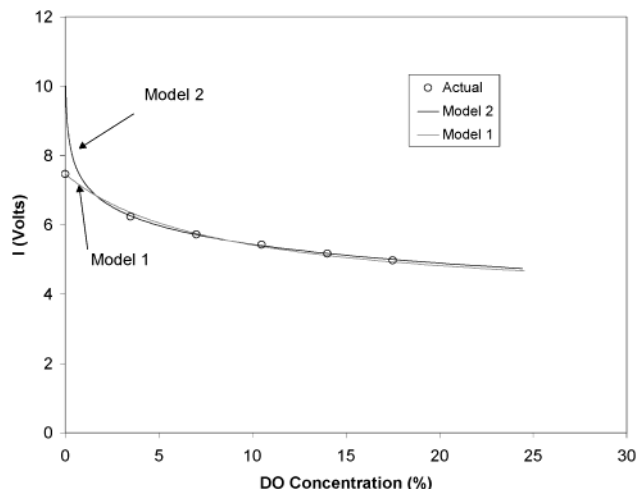


**Figure 5.** Plot of signal as a function of DO concentration (oxygen saturation) obtained from Models 1 and 2 based on calibration data from the oxygen sensor after four autoclave cycles. The circles represent actual values. Only the lower region of DO concentrations is shown.

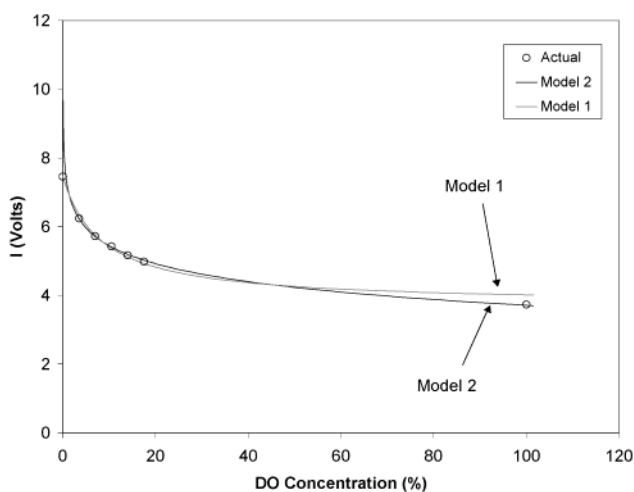


**Figure 6.** Plot of signal as a function of DO concentration (oxygen saturation) obtained from Models 1 and 2 based on calibration data from the oxygen sensor after four autoclave cycles. The circles represent actual values. The full range of DO concentrations is shown.

a low DO concentration range (0–24% oxygen saturation) and compares them to actual values obtained from sensor calibrations performed after four autoclave cycles. Figure 6 plots the signals calculated by Models 1 and 2 as a function of DO concentration for the complete DO concentration range (0–100% oxygen saturation) and compares them to actual values obtained from sensor calibrations performed after four autoclave cycles. These figures demonstrate that neither model is effective over the entire range of DO concentration from 0% to 100% oxygen saturation. Specifically, Model 1 is deficient at high DO concentrations (Figure 6), while Model 2 is deficient at low DO concentrations (Figure 5), i.e., the effective ranges of Models 1 and 2 are approximately 0–50% oxygen saturation and 2–100% oxygen saturation, respectively.

The reasons for the failure of the two models to accurately predict DO concentration over the entire range are mathematical in nature. Each of the models has its flaws. Model 1 (eq 3) must necessarily fail as  $I$  approaches  $I_{NQ}$ . A difficulty lies in separating signal due to interfering radiation from that due to actual quenchable fluorescence

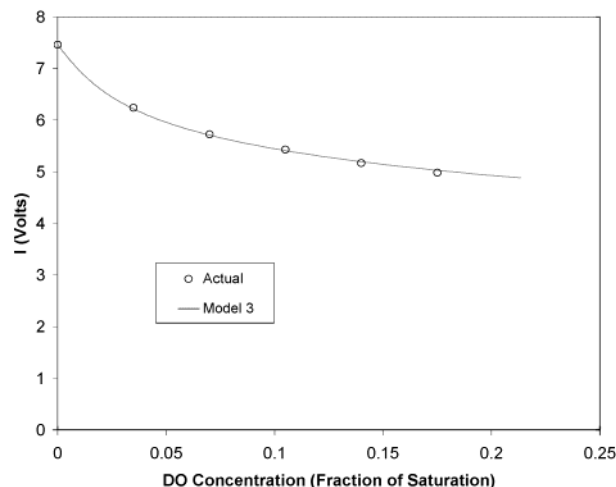


**Figure 7.** Plot of signal vs DO concentration (oxygen saturation) generated by Model 3 based on calibration data from the oxygen sensor after four autoclave cycles. The circles represent actual values. Only the portion of the DO range from 0 to air saturation is shown.

of the complex that remains unquenched at 100% oxygen saturation. Alternatively, a value for  $I_{NQ}$  that is not equal to the signal at 100% oxygen saturation as well as a value for  $K_{sv}$  can be fit to the data to improve the performance of the model and to prevent this failure at very high DO concentration. However, the cost of this better fit for the high DO concentration range is a noticeably poorer fit for low values of DO concentration. By its nature, Model 1 cannot accurately model DO concentration over its full range. The failure of Model 2 (eq 4) is due to the fact that the natural logarithm of  $[Q]$  approaches  $-\infty$  as  $[Q]$  approaches 0 from the positive direction. The result is that, in the limit, the values of  $I$  required by the model to predict  $[Q]$  become exponentially large. In reality, when the model is applied to actual data, values from the oxygen sensor cannot exceed  $I_0$ . As a result, the model over predicts the actual DO concentration in the vicinity of  $I_0$ . The amount of over prediction in this region is not large in terms of magnitude but is large in terms of percentage error when compared to the actual value.

As a result of the deficiencies in Models 1 and 2, the following modeling equation was developed to fit the sensor data over the full DO concentration range:

$$Q = \exp\left(\frac{I - I_{sat}}{\eta(I_0 - I_{sat})}\right) - \exp\left(\frac{I_0 - I_{sat}}{\eta(I - I_{sat})}\right) \quad (5)$$

where  $I$  is the signal from the oxygen sensor,  $I_0$  is the signal in the absence of oxygen,  $I_{sat}$  is the signal at oxygen saturation in the fluid,  $\eta$  is a constant determined from the calibration data, and  $Q$  is the fraction of oxygen saturation given by

$$Q = \frac{[Q]}{[Q]_{sat}} \quad (6)$$

Equation 5 will subsequently be referred to as Model 3. This model was empirically derived on the basis of calibration data obtained and is not based on known physical correlations. Comparison of this model to actual data from calibrations performed after four autoclave cycles is shown in Figures 7 and 8. Figure 7 is a plot of  $I$  vs  $Q$  generated by eq 5 for the DO range from 0% to 100% air saturation compared with actual values obtained from calibrations performed after four autoclave

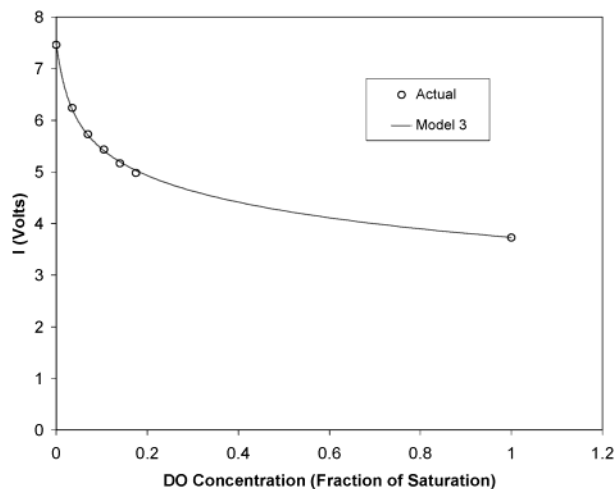


**Figure 8.** Plot of signal vs DO concentration (oxygen saturation) generated by Model 3 based on calibration data from the oxygen sensor after four autoclave cycles. The circles represent actual values. The complete range of DO concentrations is shown.

cycles. Figure 8 is a plot of  $I$  vs  $Q$  generated by eq 5 for the DO range from 0% to 100% oxygen saturation compared with actual values obtained from calibrations performed after four autoclave cycles. These plots show that Model 3 is capable of predicting DO concentration with good accuracy over the entire range of DO concentration from 0% to 100% oxygen saturation in the fluid. It is worth noting that the  $\eta$  calculated for Model 3 changed very little from the calibration performed on the unautoclaved sensor to the calibration performed on the sensor after four autoclave cycles. Over this period,  $\eta$  changed from  $-0.2018$  to  $-0.1996$  or  $-1.1\%$ . This suggests that  $\eta$  is a descriptor of the properties of  $[\text{Ru}(\text{dpp})_3]^{2+}$  fluorescence quenching in the silicone polymer matrix and lends support to the theory that the distribution of modes of fluorescence quenching is unaltered by autoclaving. The utility of this relationship is as follows. If  $\eta$  is invariant, then oxygen concentration can be accurately modeled over the full range of DO concentration from 0% to 100% oxygen saturation in the fluid by only performing calibrations to determine  $I_0$  and  $I_{\text{sat}}$ . If  $I_0$  and  $I_{\text{sat}}$  are stable over a long period of time, calibration need then only be performed periodically.

**Operation of Modified HARV.** The completed system, consisting of HARV system, oxygen sensing unit, mass flow controllers, and computer for data acquisition and process control was assembled and tested in an incubator at  $27^\circ\text{C}$  to determine how the parts of the system function together as a whole. The oxygen sensor headpiece was calibrated at  $27^\circ\text{C}$  prior to assembly in the HARV for autoclaving. This sensor was subjected to over 10 autoclave cycles prior to conducting the cell culture experiments described here. A cell culture run was conducted with uninfected *S. frugiperda* Sf-9 (Sf-9) cells. Cells in the HARV showed good growth, increasing exponentially from  $1 \times 10^6$  cells/mL at seeding to  $7 \times 10^6$  cells/mL at which time growth became nonexponential.

Overall, monitoring of the DO concentration worked well and development of the control system is improving. Figure 9 shows the performance of the control system in response to changes in the DO setpoint. The experiment was performed with a culture of Sf-9 cells in the HARV at a density of  $(2-3) \times 10^6$  cells/mL. The experiment was carried out in an incubator at  $27^\circ\text{C}$  where the vessel was

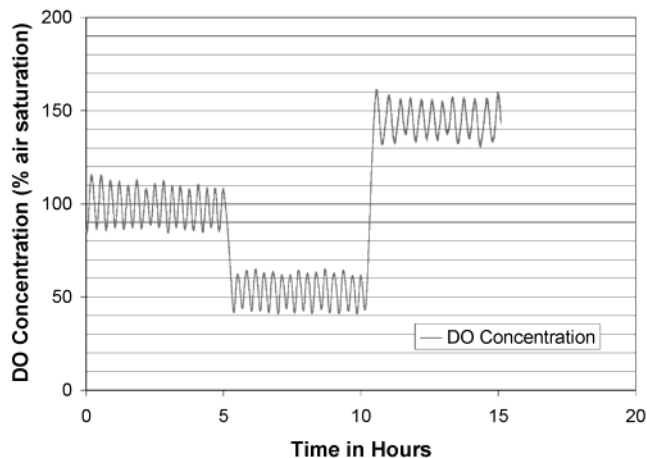


**Figure 9.** Plot of DO concentration (air saturation) as a function of time for a culture of Sf-9 cells grown in the HARV bioreactor. The data show the ability of the current control system to respond to changes of the DO setpoint from 100% to 50% to 150% air saturation. The decrease in DO concentration from 100% to 50% was obtained by allowing cellular  $\text{O}_2$  consumption, and the increase from 50% to 150% was accomplished by increasing the  $\text{O}_2$  flow to the HARV.

surrounded by ambient air. Figure 9 shows the potential for accurate DO concentration control in the HARV. A good response to setpoint changes is indicated, as well as the ability to hold a constant value within a range of approximately  $\pm 10\%$  air saturation. The corresponding off-sets were essentially symmetrical around the 100% air saturation setpoint, with the range more heavily skewed toward 100% air saturation for the 50% and 150% air saturation setpoints. Difficulties in control lie in the time required for oxygen diffusion through the silicone membrane of the HARV vessel, diffusion/mixing inside the vessel, and response time of the oxygen sensor. The thicknesses of the silicone oxygenation membrane ( $\sim 180 \mu\text{m}$ ) and layers on the oxygen sensor ( $\sim 300 \mu\text{m}$  total thickness (sensing chemistry layer + black protective layer) prior to drying) are comparable. Therefore, it would be reasonable to assume that the diffusion times and therefore the corresponding lag times are similar for oxygen diffusion through the silicone membrane and for sensor response. Computational fluid dynamics (CFD) studies will provide the means to attain a reasonable estimation of the lag time due to oxygen diffusion inside the vessel.

It was determined that the error in the DO concentration measurements was less than 3% air saturation on the basis of comparing the calibration curves obtained prior to autoclaving to those obtained following a bioreactor run. This is an acceptable error for general bioreactor monitoring and control. Contributions to this error may include (i) sensor changes during autoclaving (which, as discussed above, have been demonstrated to be relatively small following exposure to three to four autoclave cycles), (ii) calibration at conditions slightly different than actual bioreactor conditions (e.g., any change in temperature can affect the signal), and/or (iii) sensor changes during the bioreactor run. More trials need to be conducted to determine the relative contribution of these factors to errors in the sensor measurements and the potential contribution of other factors. It has been clearly demonstrated, however, that this probe-type oxygen sensor can accurately monitor the DO concentration and provides the means for DO concentration control within the HARV.

## Conclusions

A dissolved oxygen probe utilizing a radioluminescent-based light source and ruthenium-based sensing chemistry has been demonstrated to be stable and capable of monitoring the dissolved oxygen (DO) concentration in a high aspect ratio vessel (HARV). In addition, the information provided by this sensor was used in conjunction with a control scheme to demonstrate the ability for DO concentration control within the HARV. Several improvements, such as the casting of a thinner sensor membrane to improve response time and the development of a control system with the ability to learn and modify its behavior, will result in a HARV with tighter control of the DO concentration around its setpoint. These modifications will allow for more meaningful cell culture experiments to be conducted in the HARV by providing a well-defined environment in terms of the DO concentration. Furthermore, it is anticipated that results of computational fluid dynamics (CFD) studies currently underway in our laboratory will provide information to operate the modified HARV in a manner to minimize DO concentration heterogeneities (e.g., by periodically changing rotational direction to induce mixing), while maintaining an environment that is conducive to the formation of 3-D cell aggregates.

## Acknowledgment

The authors acknowledge the support of NASA (NAG8-1591 and NAG8-1592). In addition, the authors thank Mike Miller, Dean Macken, and Herb Dircks for their assistance in constructing the oxygen sensor and HARV.

## References and Notes

- Low, H. P.; Savarese, T. M.; Schwartz, W. J. Neural precursor cells from rudimentary tissue-like structures in a rotating-wall vessel bioreactor. *In Vitro Cell. Dev. Biol.: Anim.* **2001**, *37*, 141–147.
- Qiu, Q. Q.; Ducheyne, P.; Ayyaswamy, P. S. 3D bone tissue engineered with bioactive microspheres in simulated microgravity. *In Vitro Cell. Dev. Biol.: Anim.* **2001**, *37*, 157–165.
- Cameron, D. F.; Hushen, J. J.; Nazian, S. J. Formation of insulin-secreting, Sertoli-enriched tissue constructs by microgravity coculture of isolated pig islets and rat Sertoli cells. *In Vitro Cell. Dev. Biol.: Anim.* **2001**, *37*, 490–498.
- Chuang, H.; Arnold, M. A. Radioluminescent sources for optical chemical sensors. *Pure Appl. Chem.* **1999**, *71*, 803–810.
- Reece, J. S.; Miller, M. J.; Arnold, M. A.; Waterhouse, C.; Delaplaine, T.; Cohn, L.; Cannon, T. Continuous oxygen monitoring of mammalian cell growth on space shuttle mission STS-93 with a novel radioluminescent oxygen sensor. *Appl. Biochem. Biotechnol.* **2003**, *104*, 1–11.
- Bambot, S. B.; Holavanahali, R.; Lakowicz, J. R.; Carter, G. M.; Rao, G. Phase fluorometric sterilizable optical oxygen sensor. *Biotechnol. Bioeng.* **1994**, *43*, 1139–1145.
- Chuang, H.; Arnold, M. A. Radio-luminescent light source for optical oxygen sensors. *Anal. Chem.* **1997**, *69*, 1899–1903.
- Van Houten, J.; Watts, R. J. Temperature dependence of the photophysical and photochemical properties of the tris-(2,2'-bipyridyl)ruthenium(II) ion in aqueous solution. *J. Am. Chem. Soc.* **1976**, *98*, 4853–4858.
- Demas, J. N.; DeGraff, B. A. On the design of luminescence based temperature sensors. *SPIE* **1992**, *1796*, 71–75.
- Chang, Q.; Randers-Eichhorn, L.; Lakowicz, J. R.; Rao, G. Steam-sterilizable fluorescence lifetime-based sensing film for dissolved carbon dioxide. *Biotechnol. Prog.* **1998**, *14*, 326–331.
- Demas, J. N.; DeGraff, B. A. Luminescence-based sensors: microheterogeneous and temperature effects. *Sens. Actuators, B* **1993**, *11*, 35–41.
- Demas, J. N.; DeGraff, B. A.; Xu, W. Modeling of luminescence quenching-based sensors: comparison of multisite and nonlinear gas solubility models. *Anal. Chem.* **1995**, *67*, 1377–1380.
- Hartmann, P.; Leiner, M. J. P.; Lippitsch, M. E. Luminescence quenching behavior of an oxygen sensor based on a Ru(II) complex dissolved in polystyrene. *Anal. Chem.* **1995**, *67*, 7, 88–93.
- Klimant, I.; Wolfbeis, O. S. Oxygen-sensitive luminescent materials based on silicone-soluble ruthenium diimine complexes. *Anal. Chem.* **1995**, *67*, 7, 3160–3166.
- Lippitsch, M. E.; Draxler, S. Luminescence decay-time-based optical sensors: principles and problems. *Sens. Actuators, B* **1993**, *11*, 97–101.
- Sacksteder, L.; Demas, J. N.; DeGraff, B. A. Design of oxygen sensors based on quenching of luminescent metal complexes: effect of ligand size on heterogeneity. *Anal. Chem.* **1993**, *65*, 3480–3483.
- Watkins, A. N.; Wenner, B. R.; Jordan, J. D.; Xu, W.; Demas, J. N.; Bright, F. V. Portable, low-cost, solid-state luminescence-based O<sub>2</sub> sensor. *Appl. Spectrosc.* **1998**, *52*, 750–754.
- Moreno-Bondi, M. C.; Wolfbeis, O. S.; Leiner, M. J. P.; Schaffar, B. P. H. Oxygen optrode for use in a fiber-optic glucose biosensor. *Anal. Chem.* **1990**, *62*, 2377–2380.

Accepted for publication March 27, 2003.

BP0257574